ACS OMEGA

http://pubs.acs.org/journal/acsodf

Article

Environmentally Benign Water-Soluble Sodium L-2-(1-Imidazolyl) Alkanoic Acids as New Corrosion Inhibitors for Mild Steel in Artificial Seawater

Jiyaul Haque, Mohammad F. Ridwan Zulkifli,* Nabilah Ismail, Mumtaz A. Quraishi, Mohd Sabri Mohd Ghazali, Elyor Berdimurodov, and Wan Mohd Norsani Bin Wan Nik*

Cite This: *ACS Omega* 2023, 8, 24797−24812

Read Online

ACCESS | Metrics & More | Article Recommendations | Supporting Information

ABSTRACT: Three novel natural amino acid-derived sodium L-2-(1-imidazolyl) alkanoic acids (IZSs), namely, sodium 2-(1H-imidazol-1-yl)-4-methylpentanoate (IZS-L), sodium 2-(1H-imidazol-1-yl)-3-phenylpropanoate (IZS-P), and sodium 2-(1H-imidazol-1-yl)-4-(methylthio)butanoate (IZS-M), were investigated as corrosion inhibitors. The IZSs were synthesized following the green chemistry principles, and their structure was characterized using FTIR and NMR techniques. The corrosion study results reveal that a moderate concentration of IZSs (having low solution conductivity) showed potential corrosion inhibition for mild steel in artificial seawater. At longer immersion, IZS-P forms a uniform protective film and exhibits the potential inhibition efficiency of 82.46% at 8.4 mmol L^{-1}. Tafel polarization results reveal that IZS-P and IZS-M act as mixed types with an anodic predominantly corrosion inhibitor. The electrochemical impedance spectroscopy results signify that IZSs inhibit mild steel corrosion through the formation of an inhibitor film on the metal surface, which was further confirmed by the FTIR, SEM, EDX, and XPS studies. DFT result shows that in IZS-P, the benzylic group ($-CH_2-Ph$) has greater electron distribution compared to isobutyl ($-CH_2CH(CH_3)_2$) in IZS-L and methythioethyl group ($-CH_2CH_2SCH_3$) which supported the corrosion inhibition performance at longer immersion [IZS-P (82.46%) > IZS-M (67.19%) > IZS-L (24.77%)].

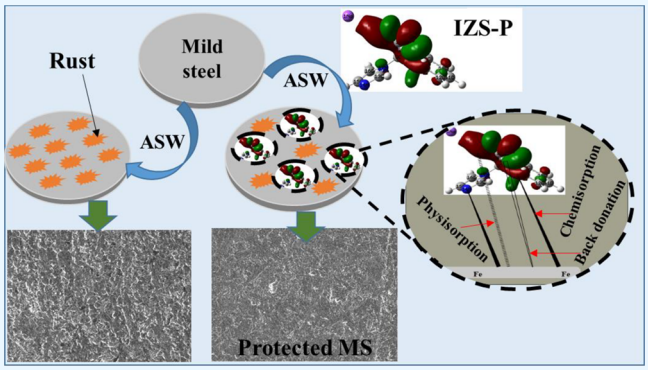

■ INTRODUCTION

Mild steel is the cheapest metal for construction with good mechanical properties, and therefore, it is widely used as a structural material in shipping, production, and mining. However, mild steel is very susceptible to corrosion in seawater which comes in contact with several applications of seawater: cooling systems, water transport, storage reservoirs, inject systems, and so forth. Consequently, corrosion causes a catastrophic effect: huge economic loss, human safety, and water pollution.[1] In practice, a chemical inhibitor is the most prominent method to prevent the corrosion of metals in corrosive media.[2]

In the past, for controlling seawater metal corrosion, a variety of inorganic inhibitors have been used such as chromates, borate, molybdates, nitrites, phosphates, and so forth. However, owing to their toxicity, most of these inhibitors are restricted to use at the commercial level. Nevertheless, nitrite-based inhibitors are still used due to their low cost and high effectiveness compared to other inorganic inhibitors.[3−5] Besides aquatic toxicity, sodium nitrate is also used as a pharmacological suicide agent.[6] Heterocyclic-based organic inhibitors have been found to be less toxic in nature; therefore, it is widely used to replace the highly toxic inorganic corrosion inhibitors. However, due to low solubility in seawater, organic compounds generally show poor inhibition efficiency or they require very high inhibitor dosage.[7−9] In this regard, mixing of an organic compound with an inorganic salt has found significantly good inhibitor efficiency compared to organic compound used alone.[10−15]

To avoid the use of inorganic salts and overcome the poor solubility and low inhibition performance of organic inhibitors in seawater, researchers focus on developing inorganic metal-based organic salts. Mor et al. reported that zinc gluconate is well soluble in seawater compared to gluconic acid and exhibited IE 84% at 5×10^{-4} M.[16] From polarization results, zinc gluconate acts as a cathodic-type inhibitor. Loto et al.

Received: January 17, 2023
Accepted: June 1, 2023
Published: July 5, 2023

ACS Publications

© 2023 The Authors. Published by American Chemical Society

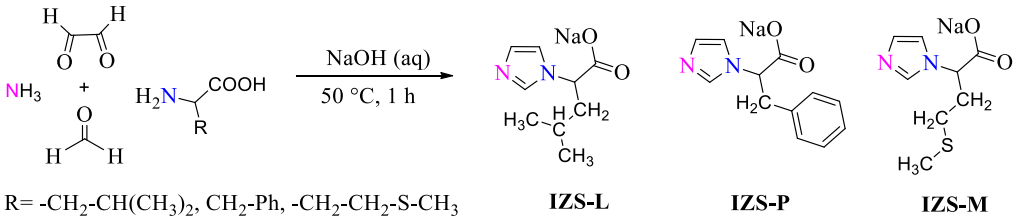

Figure 1. Synthesis scheme of inhibitors.

studied the corrosion inhibition effect of calcium gluconate on mild steel in artificial seawater.[17] Calcium gluconate showed almost similar inhibition to zinc gluconate, but the inhibition behavior of calcium gluconate was opposite predominant anodic inhibitor. Besides low toxicity, the search for organic corrosion inhibitors which have ease of synthesis and are cost effective is still a challenge.

For the development of environmentally benign potential inhibitors along with an understanding of the inhibition mechanism, heterocyclic compounds have been considered a great alternative to replace the toxic inorganic corrosion inhibitors.[15,18−21] Recently, researchers have concentrated more on imidazole-based compounds due to their simple structure and very high adsorption affinity with carbon steel and copper metal in acid as well as in alkaline media, resulting in effective corrosion inhibition at a low inhibitor dose.[22−26] Curkovic et al. found that the imidazole compound exhibited better adsorption in an alkaline medium compared to an acidic medium.[24] Recently, our research group disclosed that the phenyl and methionine amino acids derived from imidazolium zwitterions showed pronounced corrosion inhibition performance compared to other similar inhibitors.[25,26] In the continuous study, in the present work, three sodium L-2-(1-imidazolyl) alkanoic acids (IZSs) have been selected as corrosion inhibitors for mild steel corrosion in a seawater environment. Imidazole-based compounds are considered less toxic than traditional corrosion inhibitors.[27] IZSs have been synthesized by simple multicomponent reactions using amino acids and other less toxic chemicals with high yield and good green metrics (high atom economy and low *E*-factor).[28] IZSs are secondary products in the pharmaceutical industry[29] and an intermediate component for the production of less toxic ionic liquid solvents.[28] Their corrosion inhibition performance and inhibition mechanism have been studied by employing electrochemical and surface characterization and DFT methods.

■ EXPERIMENTAL SECTION

Material and Electrolyte. The required chemicals were purchased from Sigma Aldrich and other companies in analytically pure form and used without further purification. The corrosion study was performed on mild steel specimens which have the following composition (wt %) C: 0.040, Si: 0.01, Mn: 0.26, P: 0.013, S: 0.004, Cu: 0.01, Ni: 0.01, Cr: 0.01, Al 0.039, N: 0.0001, remaining balanced Fe. The mild steel sample was cut in specific sizes of dimensions 20.3 × 20.3 × 0.9 mm for all analyses. For the electrochemical study, 1 cm^2 surface of mild steel was exposed to an electrolyte using a flat corrosion cell. The mild steel coupons were polished uniformly through a Forcipol 300-1 V grinder and polisher instrument using different grades of silica sand papers (from 180 to 1500). Then, the coupons were cleaned with distilled water, degreased in acetone, and finally dried and stored in the desiccator.

The electrolyte artificial seawater (ASW) was prepared by following the ASTM standard.[30] Different concentrations in the range of 2.1 to 10.5 mmol $L^{-1}$of inhibitor solution were prepared in ASW solution.

Inhibitor Synthesis. The synthesis was carried out by mixing formaldehyde (5.70 mL, 36% w/v) and glyoxal solution (4.10 mL, 32% w/v) in a 150 mL round bottle flask.[28] The reaction mixture was heated up to 50 °C. Then, a mixture of the amino acid (0.04 mol L^{-1}), ammonium solution (4.8 mL, 28% w/v), and an aqueous solution of NaOH (14.4 mL, 10% w/v) was added to the reaction mixture and heated at 50 °C for 4 h. After the reaction, the unreacted formaldehyde and glyoxal were washed out with ether, and the remaining solvent was removed under reduced pressure. The obtained compounds were dried by freeze drying and then finally kept in a desiccator containing a phosphorous pentoxide drying agent. The synthesis scheme is represented in Figure 1.

The structures of synthesized compounds were characterized by the FTIR and NMR (^{1}H and ^{13}C NMR) techniques. FTIR analysis was conducted by a Bruker instrument, and NMR analysis was carried out using a Bruker Advance III, 400 MHz spectrometer.

Corrosion Study. *Electrochemical Measurement.* The electrochemical behavior of corrosion inhibitors was determined by linear polarization resistance (LPR), electrochemical impedance spectroscopy (EIS), and Tafel polarization studies in ASW (pH 8.2) at 24 ± 2 °C. A Gamry 1010E potentiostat/galvanostat workstation was used to perform the electrochemical experiments with a commercial three-electrode flat corrosion cell assembly that included 1 cm^2 exposed surface area of mild steel (as a working electrode), an Ag/AgCl electrode (as a reference electrode) and a platinum rod (as a counter electrode). A range of inhibitor concentrations, 2.1 to 10.5 mmol L^{-1}, were used to determine the optimum concentration of inhibitors.

Before each experiment, the mild steel as a working electrode was immersed in the test solution for 3 h to establish the steady state of open-circuit potential (E_{OCP}). LPR measurement is a fast technique to elucidate the corrosion rate within a shorter period (10 min). LPR was carried out by polarization of the working electrode in the range of −20 to +20 mV at E_{OCP} by applying a scan rate of 0.167 mVs^{-1}. The polarization resistance (R_p) was determined from the slope values, which were obtained by fitting the potential versus current density curve. EIS measurements were performed in the frequency range 0.01 Hz to 100 kHz with a sinusoidal voltage signal 10 mV peak to peak at the respective E_{OCP}. Tafel polarization measurements were performed by applying a range of potential −250 to +250 mV at E_{OCP} with a swipe rate of 0.5 mVs^{-1}. The experiments were repeated to obtain reproducible results. Gamry Echem analyst 5.0 software was used to analyze the LPR, EIS, and Tafel polarization results.

https://doi.org/10.1021/acsomega.3c00366
ACS Omega 2023, 8, 24797−24812

Surface Analysis (FTIR, SEM, EDX, and XPS). The surface analysis was carried out on mild steel after 14 days immersion in ASW in the absence and presence of the inhibitor. The FTIR spectra were recorded at ATR sampling mood using the Bruker instrument. The Scanning electron microscopy (SEM) and Energy Dispersive X-Ray (EDX) analysis were carried out using a JEOL 6360LA instrument by applying at 10 kV potential and scanning at 1,000 X magnification. The auto fine coater JFC-1600 was used for coating before SEM analysis. X-ray photoelectron spectrophotometer (XPS) analysis was carried out using XPS AMICUS, Kratos Analytical, A Shimadzu instrument and Mg-Kα (1253.6 eV) was used as an X-ray source for the excitation of samples. The XPS spectra of all elements were referenced to the binding energy of 284.6 eV of C 1s peak of carbon. XPSPEAK41 software was used to analyze the XPS data.

Corrosive Solution Analysis. The Corrosive solution analysis was conducted before and after 24 h immersion in ASW. UV−visible analysis was done using an UV-800 Shimadzu UV spectrometer. The pH and solution conductivity were measured using a Mettler Toledo pH and conductivity meter.

DFT Study. The electronic parameters and orbital information of IZSs were studied by quantum chemical calculations using Gaussian 09 software.[31] The calculations were carried out by the DFT method by applying a higher basic set, B3LPY/6-31(d,p). Gauss View 5.0 software was used to input the files and view the structure and geometry of optimized inhibitor molecules. The calculations of neutral molecules of inhibitors were done in gaseous and aqueous media, and the effect of water molecules was modeled using the internal equation formalism polarization continuum model.

In the calculations, first, the optimization of molecules was done to get a stable lowest energy structure, and then the frontier molecular orbital energy was calculated: energy of highest occupied molecular orbitals (E_{HOMO}) and energy of the lowest unoccupied molecular orbitals (E_{LUMO}). Energy gap (ΔE), absolute hardness (η), absolute softness (σ), and absolute electronegative (χ) were calculated by using the following equations:

$$\Delta E = E_{LUMO} - E_{HOMO} \tag{1}$$

$$\eta = \frac{1}{2}(E_{LUMO} - E_{HOMO}) \tag{2}$$

$$\sigma = \frac{1}{\eta} \tag{3}$$

$$\chi = -\frac{1}{2}(E_{LUMO} - E_{HOMO}) \tag{4}$$

Another important parameter, the fraction of electron transfers (ΔN) from the inhibitor molecule to the metal surface, is calculated by the equation

$$\Delta N = \frac{\chi_{metal} - \chi_{inh}}{2(\eta_{metal} + \eta_{inh})} \tag{5}$$

It was found by researchers[32−34] that in the calculation of ΔN, more appropriate results were obtained by using the work function (φ) for the metal in place of electronegativity. Thus, using φ in place of χ, eq 5 became eq 6 for the Fe metal.

$$\Delta N = \frac{\varphi_{Fe} - \chi_{inh}}{2(\eta_{Fe} + \eta_{inh})} \tag{6}$$

For bulk iron, the theoretical value of $\eta_{Fe} = 0$ was used. In the present work, the φ calculated value of Fe is 4.82 eV.[21]

RESULTS AND DISCUSSION

Green Chemistry Metrics and Characterization of Synthesized Inhibitors. The three sodium L-2-(1-imidazol-yl) alkanoic acids were synthesized using nontoxic chemicals having high LD50 (oral rat) values (>300 mg/kg). The synthesis was performed through a multicomponent reaction method at low temperatures in water (as a greener solvent). Multicomponent reaction facilitates two important green chemistry metrics: high atom economy (AE) and low *E*-factor (low waste), resulting in around 99% product yield, as shown in Table S1. The AE is associated with the number of atoms used in the reactants that are present in products. The obtained AE for all three IZS inhibitors was close to 80% (Table S1). This indicated that a maximum number of reactant atoms get associated with the synthesized inhibitors. The *E*-factor (green parameter) is related to the amount of waste generated per kg of inhibitor synthesis. The calculated *E*-factor s were between 1.394 and 1.742 g. The obtained *E*-factor is acceptable for the production of corrosion inhibitors.[35,36]

The characterization FTIR and NMR spectra of the synthesized inhibitors depicted in Figures S1 and S2 and their spectral data are described below:

IZS-L, Sodium 2-(1H-imidazol-1-yl)-4-methylpentanoate

FTIR-ATR (ν_{max}/cm^{-1}): 3114 (=C−H), 2962 (−C−H), 1603 (−COO, asymmetric), 1501 (C=C) 1373 (−COO, symmetric), 1076 (C=C), 742 (=C−H, bend), **^{1}H NMR** (400 MHz, D2O) δ (ppm): 0.77−0.80 (d, 3H), 0.82−85 (d, 3H), 1.14−1.25 (m, 1H), 1.80−1.96 (m, 2H), 4.74−4.77 (dd, 1H), 7.12−7.16 (d, 1H), 7.26 (s, 1H), 8.06−8.13 (d, 1H)′ **^{13}C NMR** δ (ppm): 20.40, 22.01, 24.42, 62.11, 120.38, 123.51, 136.08, 176.70.

IZS-P, Sodium 2-(1H-imidazol-1-yl)-3-phenylpropanoate

FTIR-ATR (ν_{max}/cm^{-1}): 3397 (O−H), 3122 (=C−H), 1598 (−COO, asymmetric), 1493 (C=C) 1374 (−COO, symmetric), 1075 (C=C), 696, 520 (phenyl).

^{1}H NMR (400 MHz, D2O) δ (ppm): 3.11−3.17 (dd, 1H), 3.41−3.46 (dd, 1H), 4.92−4.96 (dd, 1H), 7.00−7.72 (d, 2H), 7.13−7.21 (m, 5H), 7.83 (s, 1H). **^{13}C NMR** δ (ppm): 38.73, 65.05, 120.35, 120.44, 123.52, 126.99, 128.70, 129.10, 129.32, 136.30, 136.90, 175.06.

IZS-M, Sodium 2-(1H-imidazol-1-yl)-4-(methylthio)-butanoate

FTIR-ATR (ν_{max}/cm^{-1}): 3114 (=C−H), 2917 (−C−H), 1603 (−COO, asymmetric), 1497 (C=−C) 1374 (−COO, symmetric), 1076 (C=C), 738 (=C−H, bend), 667 −C−S). **^{1}H NMR** (400 MHz, D2O) δ (ppm): 1.97 (s, 3H), 2.19−2.25 (m, 2H), 2.33−2.39 (t, 2H), 4.86−4.89 (t, 1H), 7.14 (s, 1H), 7.20−7.26 (d, 1H), 8.13−8.16 (d, 1H). **^{13}C NMR** δ (ppm): 13.92, 29.53, 31.23, 62.07, 120.23, 123.94, 136.41, 175.57.

LPR Measurement. In electrochemical tests, LPR techniques were used to elucidate the inhibition performance of IZSs at inhibitor concentrations in ASW. Before the LPR, open circuit potential (OCP) was run to determine the stable corrosion potential, as shown in Figure S3. From OCP, in the presence of IZS-P and IZS-M, the open circuit potential (E_{ocp}) shifted significantly toward the positive direction (noble region) compared to IZS-L. This indicates that the addition

https://doi.org/10.1021/acsomega.3c00366
ACS Omega 2023, 8, 24797−24812

of IZS-P and IZS-M effectively lowers the corrosion rate of mild steel. Furthermore, from LPR results, the calculated polarization resistance (R_p) shows that IZS-L does not significantly increase R_p values compared to IZS-P and IZS-M, as shown in Figure 2. Hence among the three inhibitors,

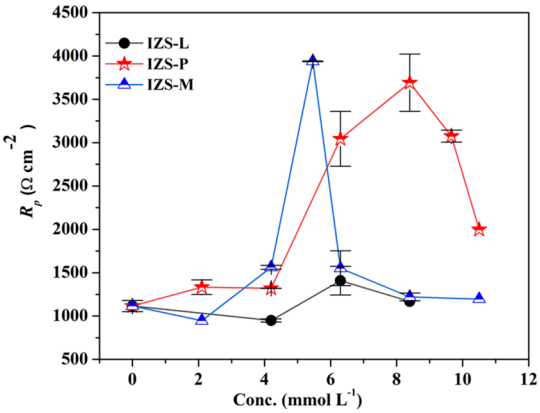

Figure 2. Polarization resistance at different concentrations of IZSs on mild steel in ASW.

IZS-L shows the lowest corrosion inhibition. From Figure 2, it can be seen that in addition to IZS-P and IZS-M, the R_p first increases, and the maximum reached is 3692 and 3989.5 Ω cm^2 at 8.40 mmol L^{-1} and 5.85 mmol L^{-1} concentration compared to blank (R_p, 1040 Ω cm^2), respectively. It indicates that inhibitors adsorb on the metal surfaces, resulting in reduced corrosion reactions. On further addition of inhibitor molecules, the R_p decreased, and it may be due to the formation of a soluble inhibitor-metal complex that increases the conductivity of the solution.[10,37]

Finally, the order of inhibition performance is IZS-L < IZS-P < IZS-M. Comparing the structure of inhibitors (see Figure 1), the presence of a side group in the imidazole ring in IZSs plays a significant role in the interaction of inhibitors with the metal d-orbital. The methionine-derived inhibitor IZS-M has a sulfur atom (soft basic nature) that can effectively donate its lone pair of electrons to iron (soft acidic nature) vacant d-orbital, whereas the phenyl alanine-derived IZS-P has π-electron in the phenyl group that can interact with the metal d-orbital. The third one is isoleucine-derived IZS-L having only an alkane group in the side chain that can create the hydrophobicity of the metal surface.

EIS Measurement. EIS study was carried out to elucidate the capacitive behavior and resistance of mild steel surface in ASW in the absence and presence of IZSs, as shown in Figure 3a−c. EIS curves show that in the presence of inhibitor molecules, the diameter of impedance curves increased compared to blank. In addition to inhibitors, decreasing the size of Nyquist curves is directly related to a resistance that develops on the metal surface and retards the charge transfer between the electrolyte and metal interface, resulting in a slowdown of the corrosion reactions.[38] The impedance curves were slightly depressed at the real axis in the absence and presence of inhibitors, which is related to the solid electrode (mild steel) and occurs due to surface roughness and inhomogeneity on the metal surface during corrosion.[39]

In Figure 3a−c, the Nyquist plots of mild steel consist of a single capacitive loop in the absence and presence of inhibitor molecules, indicating that the corrosion mechanism was not

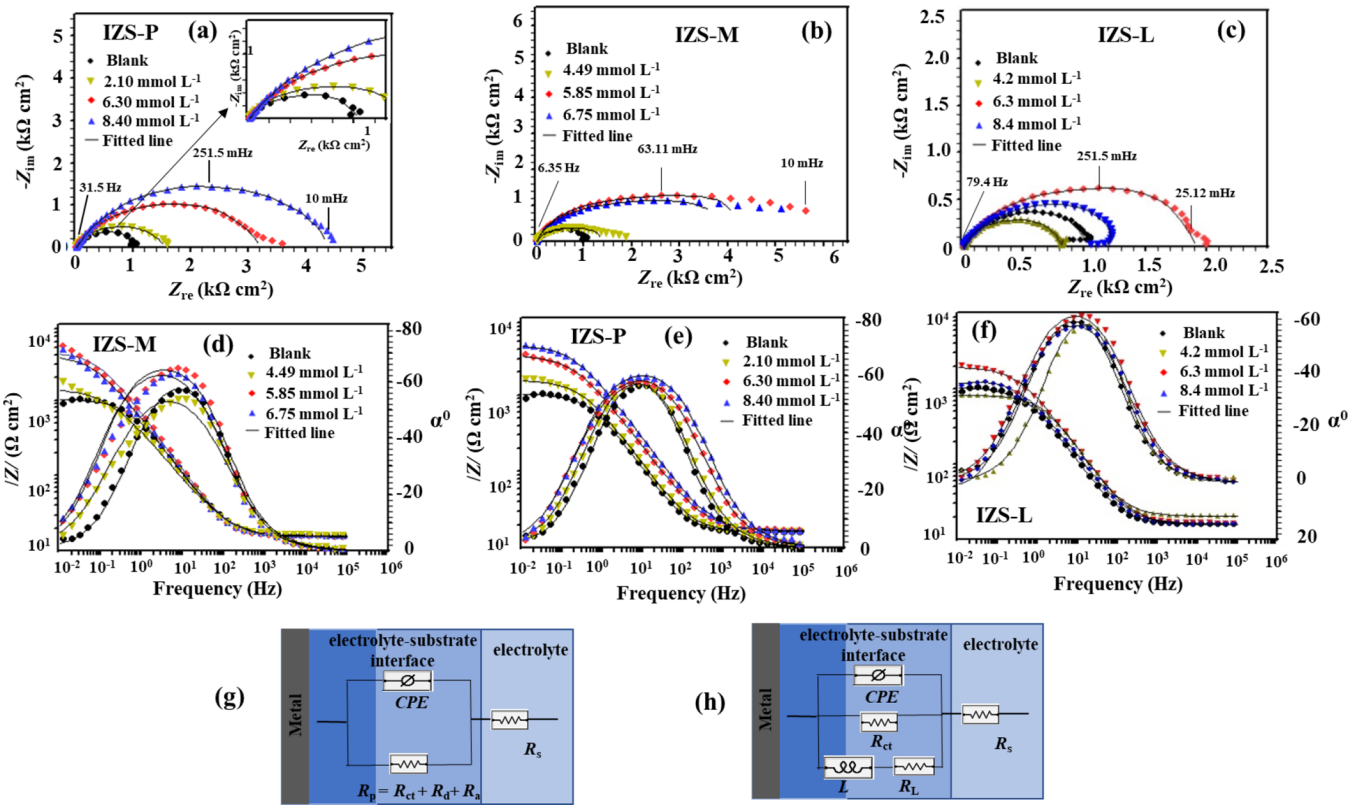

Figure 3. Nyquist (a−c) plots, bode (f vs |Z|), and phase angle (f vs α^0) plots (d−f) for mild steel in ASW without and with different concentrations of IZSs and proposed equivalent simple (g) and inductance (h) containing the electrical circuit model.

https://doi.org/10.1021/acsomega.3c00366
ACS Omega 2023, 8, 24797−24812

Table 1. EIS Parameters Obtained for Mild Steel in the Absence and Presence of IZS Inhibitor Molecules in ASW

inhibitor	conc. (mmol L^{-1})	R_s (Ω cm)	Y_0 ($\mu\Omega$ cm^2 s^{-n})	n	C_{dl} (μF)	R_p (Ω cm^2)	IE (%)	χ^2
blank	00.0	15.82	286.3	0.799	329.92	1040.0 ± 18.7		1.41×10^{-3}
IZS-P	2.10	15.79	366.3	0.750	308.52	1578.0 ± 186	34.09	6.21×10^{-6}
	6.30	16.80	239.3	0.727	224.98	3355.8 ± 248	69.01	781×10^{-6}
	8.40	16.44	176.6	0.736	156.55	4569.44 ± 675	77.24	284×10^{-6}
IZS-M	4.49	15.25	175.5	0.754	148.23	1446.0 ± 42.0	28.08	7.29×10^{-3}
	5.85	15.06	161.2	0.782	138.65	4393.21 ± 9.5	76.32	8.88×10^{-3}
	6.75	15.69	322.4	0.692	346.51	3963.0 ± 82.6	73.38	7.59×10^{-3}
IZS-L	4.20	20.31	218.6	0.805	153.20	807.9 ± 5.682	−28.72	0.73×10^{-3}
	6.30	15.89	278.0	0.757	268.52	1957 ± 16.67	46.86	1.84×10^{-3}
	8.40	15.66	365.4	0.739	333.24	1149 ± 20.30	9.48	1.12×10^{-3}

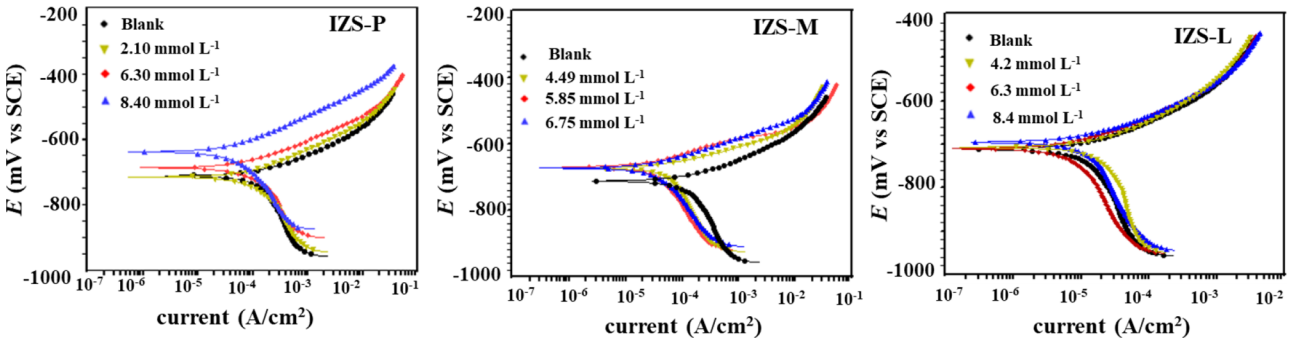

Figure 4. Tafel plots for mild steel in ASW in the absence and presence of IZSs.

changed after the addition of inhibitors. A corresponding simple equivalent circuit was used to analyze the impedance curves, as shown in Figure 3g. The validity of the circuit was confirmed by the minimum error values and the goodness of fit (χ^2), as shown in Table 1. The circuit consists of R_s (solution resistance), R_p (polarization resistance), and CPE (constant phase element). Here R_p is the total resistance that is the sum of the charge transfer resistance (R_{ct}), diffusion resistance (R_d), and accumulation resistance (R_a) ($R_p = R_{ct} + R_d + R_a$). In IZS-L, an inductive loop was obtained at 6.3 mmol L^{-1} concentration at lower frequency. This Nyquist plot was analyzed using a series of inductance (L) and inductive resistance (R_L) connected in parallel to R_{ct} and CPE, as shown in Figure 3h. In the circuit, CPE is used in place of the capacitor to obtain more accurate results. CPE can be calculated using the following equation:

$$Z_{CPE} = Y_0^{-1}(j\omega)^{-n} \tag{7}$$

where Y_0 is the admittance of CPE, j is the imaginary number ($j^2 = -1$), and ω is the angular frequency in rad/s. The parameter n is the phase shift and its values lie from −1 to 1, depending upon the surface roughness and adsorption/desorption of the inhibitor from the metal surface.[40] In addition, the adsorption of inhibitor molecules in ASW can change the charge of capacitance present on the electrolyte-metal interface. Hence, double-layer capacitance (C_{dl}) is a good parameter to explain the adsorption of inhibitors on the metal surface. The values of C_{dl} were determined using the following equation:

$$C_{dl} = Y_0(\omega_{max})^{n-1} \tag{8}$$

Using the polarization resistance (R_p) in the absence (R_p^0) and presence R_p^i of inhibitors, the inhibition efficiency (IE) was calculated using the following relationship:

$$\mathrm{IE}(\%) = \frac{R_p^i - R_p^0}{R_p^i} \times 100 \tag{9}$$

Table 1 shows that in the presence of inhibitors, mild steel shows a very high R_p compared to the blank. The highest R_p value was 4569.44, 4393.21, and 1957 Ω cm^2 in the presence of optimum concentration of IZS-P, IZS-M, and IZS-L, respectively. The corresponding inhibition efficiencies are 77.24% (8.40 mmol L^{-1}, IZS-P), 76.32% (5.85 mmol L^{-1}, IZS-M), and 46.85% (6.30 mmol L^{-1}, IZS-L). This reveals that IZS-P and IZS-M covered the greater metallic surface and minimized the electrolyte-metal interaction compared to IZS-L. The decreasing C_{dl} values in addition to IZSs indicate that the inhibitor molecule adsorbs on the metallic surface replacing preadsorbed water molecules and isolating the metal from the interaction electrolyte (containing corrosive ions).[41]

The Bode (f vs $|Z|$) and phase angle (f vs α^0) plots of EIS results of mild steel in the absence and presence of IZSs are shown in Figure 3d−f. At lower frequencies of Bode plots, the impedance modulation increases with the addition of inhibitor molecules, suggesting the formation of a protective inhibitor film on the metallic surface. Furthermore, increasing the values of the phase angle toward −90° (which means capacitive nature), indicates that inhibitors cause the smoothness of the metal by reducing the corrosion process.

Tafel Polarization Measurement. The inhibition action of IZS-P and IZS-M was further examined by the measurement of Tafel polarization on mild steel in ASW, as depicted in Figure 4. The corrosion current density decreased with the addition of inhibitors. In the presence of IZS-P, at 8.40 mmol L^{-1}, the anodic curve was more shifted compared to the cathodic curve. This indicates that IZS-P negative ions compete with chloride ions and adsorb predominantly on the metallic surface, resulting in reduced corrosion rate of mild steel, whereas

https://doi.org/10.1021/acsomega.3c00366
ACS Omega 2023, 8, 24797−24812

Table 2. Tafel Polarization Parameters for Mild Steel in the Absence and Presence of IZS Inhibitor Molecules in ASW

inhibitor	conc. (mmol L^{-1})	E_{corr} (mV/SCE)	β_a (mV/dec)	$-\beta_c$ (mV/dec)	i_{corr} (μA/cm^2)	IE (%)	θ
Blank	00.0	−712	74.10	385.2	14.8 ± 2.30		
IZS-P	2.10	−715	72.70	148.3	7.25 ± 2.30	51.01	0.5101
	6.30	−687	71.00	154.4	6.96 ± 1.68	52.97	0.5297
	8.40	−638	78.30	153.8	3.92 ± 0.15	73.51	0.7351
IZS-M	4.49	−676	51.10	152.9	5.20 ± 0.31	64.86	0.6486
	5.85	−664	50.50	156.5	2.50 ± 0.02	83.10	0.8310
	6.75	−673	59.60	171.0	3.00 ± 0.01	79.73	0.7973
IZS-L	4.20	−706	87.3	453.6	26.59	−79.66	−0.7966
	6.30	−710	65.60	253.9	7.870	46.82	0.4682
	8.40	−695	67.20	289.8	12.80	13.51	0.1351

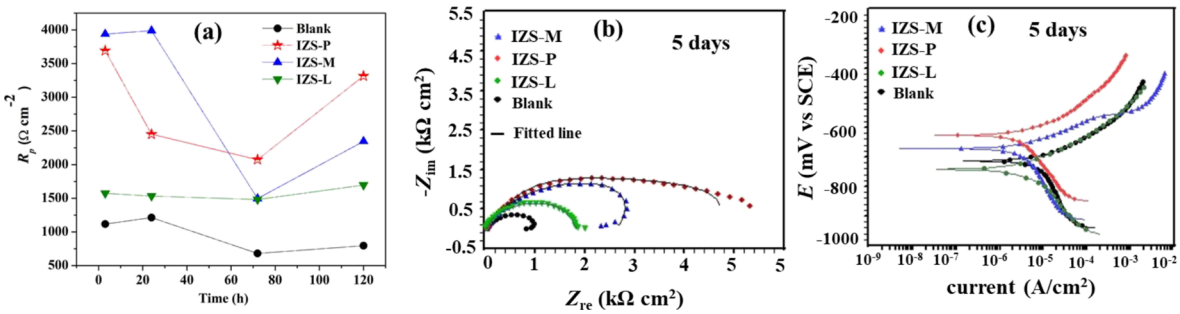

Figure 5. Variation polarization resistance with immersion time (a) and EIS (b) and Tafel (c) plots of mild steel in ASW in the absence and presence of optimum concentration IZSs.

Table 3. LPR, EIS, and Tafel Study for Mild Steel in the Absence and Presence of IZS Inhibitor Molecules in ASW after 5 Days Immersion

inhibitor	LPR		EIS					Tafel	
	R_p (Ω cm^2)	IE (%)	R_s (Ω cm)	L (Ω s cm^2)	R_p (Ω cm^2)	IE (%)	E_{corr} (mV/SCE)	i_{corr} (μA/cm^2)	IE (%)
Blank	795 ± 187		16.00	36,680	883.77 ± 187		−713	11.30 ± 1.4	
IZS-P	2916 ± 128	72.89	24.82		5064 ± 324	82.46	−648	2.65 ± 0.9	76.55
IZS-M	2346 ± 187	66.11	16.63	64,510	2693.98 ± 227	67.19	−671	3.35 ± 0.9	70.35
IZS-L	1696	53.12	22.69		1850	52.23	−741	8.5	24.77

IZS-M shifted both the anodic and cathodic curves toward lower current density. This reveals that IZS-M blocks both the anodic and cathodic active sites of the metal surface at the same time. However, IZS-L does not cause significant change in Tafel curves, revealing that IZS-L is a least effective inhibitor among the IZSs.

Table 2 shows the polarization parameters for mild steel in the absence and presence of IZSs obtained by the extrapolation of the linear portion of Tafel curves. In the presence of inhibitors, the maximum corrosion potential (E_{corr}) shifted to −638 mV/SCE (IZS-P), −664 mV/SCE (IZS-M), and −695 mV/SCE (IZS-L) compared to the blank (−712 mV/SCE). The shifted E_{corr} values toward a positive direction were less than −85 mV,[21] revealing that the studied IZSs inhibitors act as mixed types with predominantly anodic inhibitors. In comparison, IZS-P more effectively blocks the anodic sites compared to IZS-M and IZS-L. The data show that with increasing inhibitor doses, the corrosion current density (i_{corr}) decreases. This indicates that increasing the number of inhibitor molecules on the metallic surface shifts the mild steel in the noble region. The inhibition efficiency of IZSs was calculated from i_{corr} using the following equation:

$$\mathrm{IE}(\%) = \frac{i^0_{corr} - i^i_{corr}}{i^0_{corr}} \times 100 \quad (10)$$

In the equation, i^0_{corr} and i^i_{corr} represent the corrosion current density in the absence and presence of inhibitors, respectively. The maximum inhibition efficiency was obtained as 73.51, 83.10, and 46.82% in the presence of IZS-P, IZS-M, and IZS-L at optimum concentrations of inhibitors. The results are in good agreement with LPR and EIS measurements.

Effect of Immersion Time. To determine the nature of the protective film of IZSs on mild steel, nondestructive OCP and LPR measurements were carried out at different time intervals. In Figure S4, it can be seen that the OCP increases (shifted in the positive direction) with immersion time in the absence and presence of inhibitor molecules, and the maximum OCP was shifted at 72 h in case of blank and in the presence of IZS-L, whereas in the presence of IZS-P and IZS-M, the maximum shifted OCP was obtained at 24 h. On further immersion of the mild steel after 24 h, the OCP was decreased.

Similar to OCP, the polarization resistance (R_p) first decreases in the case of blank and inhibitors with immersion time up to 72 h; see Figure 5a. This reveals that the formation of a rust film cannot act as a protective layer, resulting in increased metal corrosion. On further immersion of the metal, the R_p values slightly increased in the case of blank, showing that the formation of a uniform rust film reduces the metal corrosion rate. Similar results were also obtained in the presence of the inhibitor. After 120 h (5 days), the phenyl ring

https://doi.org/10.1021/acsomega.3c00366
ACS Omega 2023, 8, 24797−24812

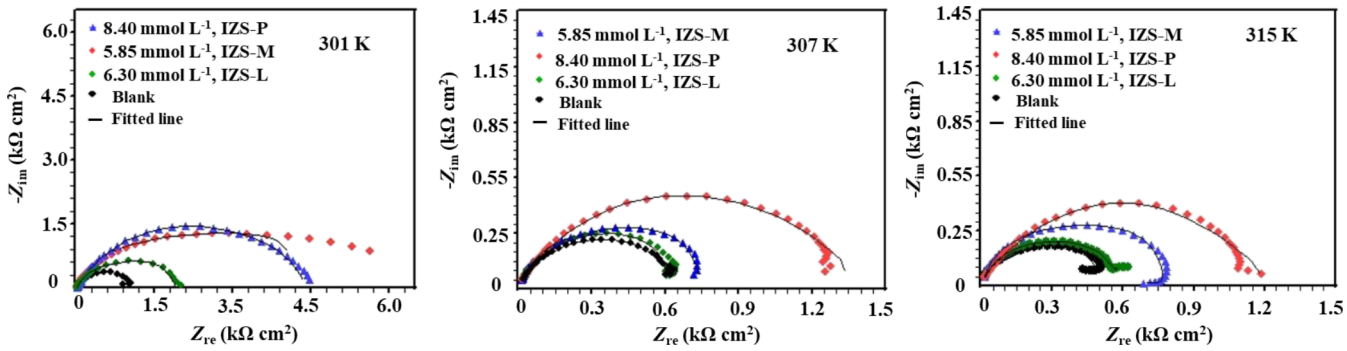

Figure 6. Variation of Nyquist plots with ASW temperature in the absence and presence of optimum concentration of IZSs.

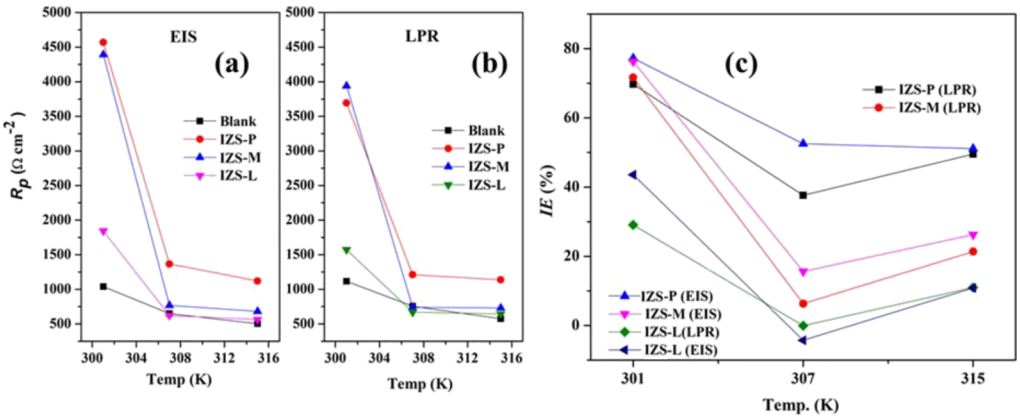

Figure 7. Effect of temperature of mild steel corrosion in the absence and presence of inhibitors: change of polarization resistance in LPR (a) and EIS (b) results and their corresponding inhibition efficiency (c).

containing IZS-P (76.02% IE) was found as a more effective inhibitor than the methylthioethyl-containing IZS-M (66.11% IE) and isobutyl-containing IZS-L (53.12%).

EIS and Tafel polarization measurements were carried out to validate the LPR results and determine the inhibition mechanism of IZS inhibitors after 5 days of immersion, as depicted in Figure 5a−c and Table 3. In Nyquist plots (Figure 5b), an inductive loop appeared at a lower frequency in blank and in the presence of IZS-M, which occurs due to the desorption of the passive oxide film.[42] These Nyquist plots were analyzed using an appropriate equivalent circuit as shown in Figure 3h. In Tafel plots (Figure 5c), the inhibitors IZS-P and IZS-M cause to shift the anodic curve significantly toward the lower current density (noble direction) compared to the blank. However, IZS-L does shift the corrosion potential (E_{corr}) toward the negative direction. Moreover, after 5 days immersion, Tafel plots (Figure 5c) were found almost similar to 3 h immersed Tafel plots (Figure 4), revealing that the longer immersion time did not change the corrosion mechanism. From Table 3, all results suggest that the IZS-P and IZS-M inhibitor films remained stable up to longer time immersion. IZS-P shows a better inhibition performance (82.46% IE) compared to IZS-M (67.3% IE) and IZS-L (24.77%).

Effect of Temperature. The effect of ASW temperature on mild steel corrosion in the absence and presence of the optimum concentration of IZSs was studied by LPR and EIS measurements. Figure S5 shows that at higher ASW temperatures, the OCP was almost stable and shifted toward the positive direction. Figure 6 shows that in all cases, the semicircle loop of Nyquist plots decreased with increasing electrolyte temperature, indicating that mild steel dissolution increases in the absence and presence of inhibitors. At all temperatures, the Nyquist plots were almost similar containing a single capacitive loop, except at 315 K in blank and in the presence of IZS-M, when an inductive loop appears at the lower frequency, which was analyzed using the well-fitted equivalent circuit, as shown in Figure 3h.

In LPR (Figure 7a) and EIS (Figure 7b) at 307 K, the polarization resistance decreased with and without inhibitors, showing the removal of rust as well as inhibitor films. However, with further increases in the temperature (up 315 K), the R_p slightly decreased. In EIS results (Figure 7b), at higher temperatures from 301 to 315 K, the R_p value significantly decreased in the presence of IZS-M (from 4393.21 to 681.2 Ω cm^2) and IZS-L (from 1957 to 563 Ω cm^2) compared to IZS-P (from 4569.44 to 1120.34 Ω cm^2). The corresponding inhibition efficiency obtained at 315 K was 52.54, 26.28, and 11.19% in the presence of IZS-P, IZS-M, and IZS-L, respectively. Hence, the temperature effect results show that IZS-P is a better inhibitor compared to IZS-M and IZS-L.

The effect of immersion time and temperature result shows that the phenyl-containing IZS-P exhibits the highest inhibition performance compared to methylthioethyl (IZS-M) and isobutyl (IZS-L) group containing the imidazole ring. Similar results were also obtained in the case of copper corrosion in neutral media[43] and in the case of mild steel corrosion in acid media.[25]

Table 4 compares the results with earlier reported work in respect of corrosion inhibition efficiency and inhibitor synthesis conditions. Simple structured inhibitor molecules either exhibit low inhibition efficiency[7−9] or require high

https://doi.org/10.1021/acsomega.3c00366
ACS Omega 2023, 8, 24797−24812

Table 4. Comparison of the Corrosion Inhibition Performance and Synthesis Condition with Earlier Reported Organic Inhibitors for Iron Alloys in Saline Environments

inhibitors	conc.	metal type	solution	inhibitor nature	IE (%)	comments	ref
N,N′-((ethane-1,2-diylbis(azanediyl))bis(ethane-2,1-diyl)) bis(quinoline-2-carboxamid	0.7 g L^{-1}	mild steel	3.5 wt % NaCl	mixed-type	72	complex structure and two step reactions with 5 h reflux	42
3-methoxypropyl-amine	8.63 g L^{-1}	X80 steel	simulated saline water	mixed-type	97	very High inhibitor dosage	41
2-thiazoline-2-thiol	0.2 g L^{-1}	carbon steel	3.5 wt % NaCl	mixed-type	62	low IE	8
acetylcysteine	0.2 g L^{-1}	carbon steel	3.5 wt % NaCl	mixed-type	54	low IE	8
1H-benzotriazole (BTA)	10 mM	mild steel	artificial sea water	mixed-type	42	low IE	7
tolyltriazole	10 mM	C15 grade steel	3 wt % NaCl	mixed-type	23	very low IE	9
diethylenetetramine (DETA) derived imidazoline	0.1 g L^{-1}	mild steel	0.5 M NaCl saturated CO_2 solutions	mixed-type with cathodic	84	Harsh reaction condition for inhibitor synthesis method (3 h reflux at 150 °C)	19
calcium gluconate	1.75%	mild steel	artificial sea water	mixed-type with anodic type	80	multi step synthesis	17
zinc gluconate	5×10^{-4} M	mild Steel	sea water	cathodic type	84	multistep synthesis	16
sodium 2-(1H-imidazol-1-yl)-3-phenylpropanoate (IZS-P)	8.4 mM/2.0 g L^{-1}	mild steel	artificial sea water	mixed-type with anodic type	82	simple structure and single step synthesis (at 50 °C for 4 h)	present work
sodium 2-(1H-imidazol-1-yl)-4-(methylthio)butanoate (IZS-M)	6.75 mM/2.0 g L^{-1}			mixed-type with anodic type	67		
sodium 2-(1H-imidazol-1-yl)-4-methylpentanoate (IZS-L)	6.30 mM/2.0 g L^{-1}			mixed-type	25		

inhibitor dosage.[44] Some of the effective corrosion inhibitors have typical synthesis method such as multistep synthesis at high temperatures and longer reaction times.[16,17,20,23] Comparing the inhibition efficiency and reaction condition, IZS-P is a potential corrosion inhibitor for mild steel corrosion in seawater.

Adsorption Isotherm. The interaction of IZS inhibitor with the mild steel surface can be determined by establishing an adsorption isotherm model. Some important adsorption isotherms, Langmuir, Frumkin, and Temkin isotherms, have been plotted using the experimentally obtained surface coverage (θ) (Table 1) and concentration of IZS, as shown in Figure 8a,b and S6. The obtained regression coefficient (R^2) was very close to 1, showing that IZS-P and IZS-L were well fitted for Langmuir adsorption isotherm (Figure 8a) and IZS-M was well-fitted for Frumkin isotherm (Figure 8b). Langmuir isotherm describes that all adsorbent sites of mild steel are identical and provide the equivalent affinity (homogeneous surface) for the adsorption of the inhibitor. Besides, there is no lateral interaction between adsorbed inhibitors, resulting in a monolayer formation of inhibitor molecules.[45] Langmuir isotherm equation is shown as

$$\frac{C}{\theta} = \frac{1}{K_{ads}} + C \tag{11}$$

where K_{ads} is the adsorption isotherm. Temkin isotherm is just a modification of Langmuir isotherm by introducing the term of surface inhomogeneity; it shows that adsorbed inhibitor molecules do not possess the lateral interaction on a solid surface (resulted in monolayer formation), but the adsorbent surface (solid surface) is not equivalent, (that is the surface is heterogeneous), resulting in the possibility to adsorption of uncharged molecules on the heterogeneous surface (chemisorption).[46] The calculated value for the IZS-M inhibitor is 1.58, which indicates that the adsorbed IZS-M molecules show a repulsive interaction on mild steel surface, and therefore the inhibition performance of IZS-M was decreased at longer immersion times and at elevated temperatures compared to IZS-P. IZS-P does not exhibit any interactions on the adsorbed mild steel surface because it follows the Langmuir isotherm, (see Figures 5 and 7). The ΔG^o_{ads} is calculated from the K_{ads} by the following equation:

$$\Delta G^o_{ads} = -RT\ln(55.5K_{ads}) \tag{12}$$

where 55.5 is the concentration of water in mol L^{-1}. The calculated ΔG^o_{ads} are −23.54, −23.58, and -15.10 kJ mol^{-1} in the presence of IZS-P, IZS-M, and IZS-L, respectively. These results show that both the inhibitor adsorb spontaneously over the mild steel surface. In addition, the adsorption mechanism based on ΔG^o_{ads} is still questionable.[47,48]

Surface Studies. *FTIR Analysis.* The interaction of the functional groups of IZS-P with mild steel surface has been studied by the analysis of FTIR spectra after immersion in 14 days in ASW, as shown in Figure 9. The mild steel (MS) spectra show different corrosion product layer peaks at 681, 536, and 442 cm^{-1} corresponding to β-FeOOH, α-Fe_2O_3, and δ-FeOOH, respectively.[49] The formation of these corrosion products reduces the metal corrosion, which was observed in immersion time LPR studies (see Figure 5a). The prominent shifting of carboxylate functional group peaks ($-COO^-$) of pure IZS-P into inhibited mild steel in AWS (IZS-P-MS) was noted from 1598 to 1628 cm^{-1} (V^a) and from 1374 to 1394

https://doi.org/10.1021/acsomega.3c00366
ACS Omega 2023, 8, 24797−24812

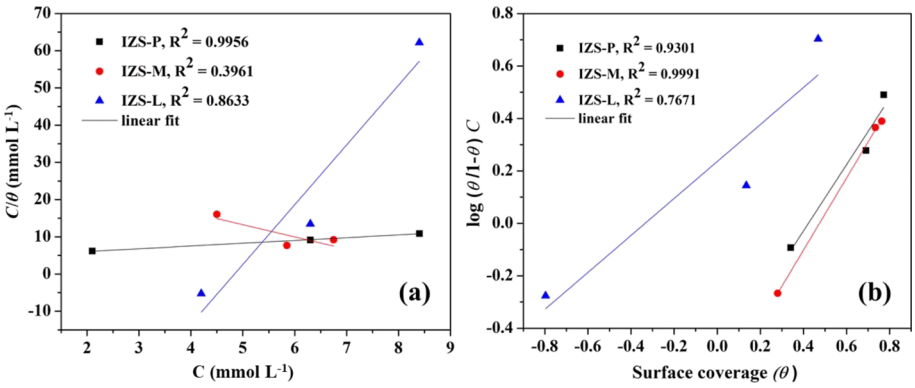

Figure 8. Langmuir isotherm (a) and Frumkin isotherm (b) of mild steel in ASW containing different concentrations of IZSs at 301 K.

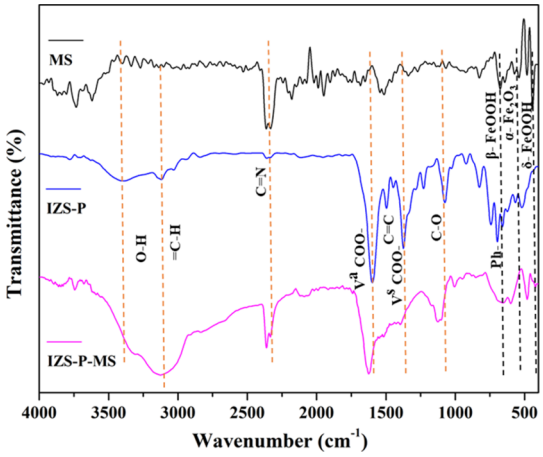

Figure 9. FTIR spectra of pure IZS-P and at 14 days immersion of mild steel in ASW without (MS) and with inhibitor (IZS-P-MS) at 301 K.

cm^{-1} (V^a). The phenyl group peaks were shifted from 696 (IZS) to 647 cm^{-1} (IZS-P-MS). The shifting of functional group peaks reveals that IZS-P effectively interacts with mild steel in ASW.

SEM/EDX Analysis. The morphological studies of inhibited and uninhibited mild steel surface were carried out by SEM analysis after 14 days and 26 days immersion in ASW, as shown in Figure 10. From the figures, the blank mild steel (in absence of inhibitor) shows uniform corrosion with high roughness compared to the polished one. In the presence of IZS-P and IZS-M, the surface smoothness significantly improved with less corrosion product compared to blank. However, the IZS-L inhibition was mild showing a much-damaged surface like blank mild steel, revealing that IZS-L does not effectively inhibit the mild steel. The high amount of corrosion product in the case of blank indicated highly corroded mild steel. Moreover, the outer oxide layer of the corrosion product is more porous, through this corrosive ion can easily diffuse and accelerate the corrosion reactions. Comparing the performance of both inhibitors after 14 days and 26 days immersion, in the case of IZS-P, the mild steel surface was significantly smoother compared to IZS-M. The better performance of IZS-P is also supported by the longer immersion study results (see Figure 5a).

The EDX results show that in the absence of an inhibitor (vide Figure S7 and Table 5), mild steel contains a significant

Table 5. EDX Elemental Composition Analysis for Mild Steel in the Absence and Presence of IZS Inhibitor Molecules in ASW after 26 Days Immersion

sample	C (at %)	O (at %)	N (at %)	Fe (at %)	S (at %)
blank	3.32	26.81		69.55	
IZS-P	2.09	0.92	0.13	96.81	
IZS-M	2.69	0.83	0.12	96.33	0.02
IZS-L	4.18	3.45	0.30	92.05	

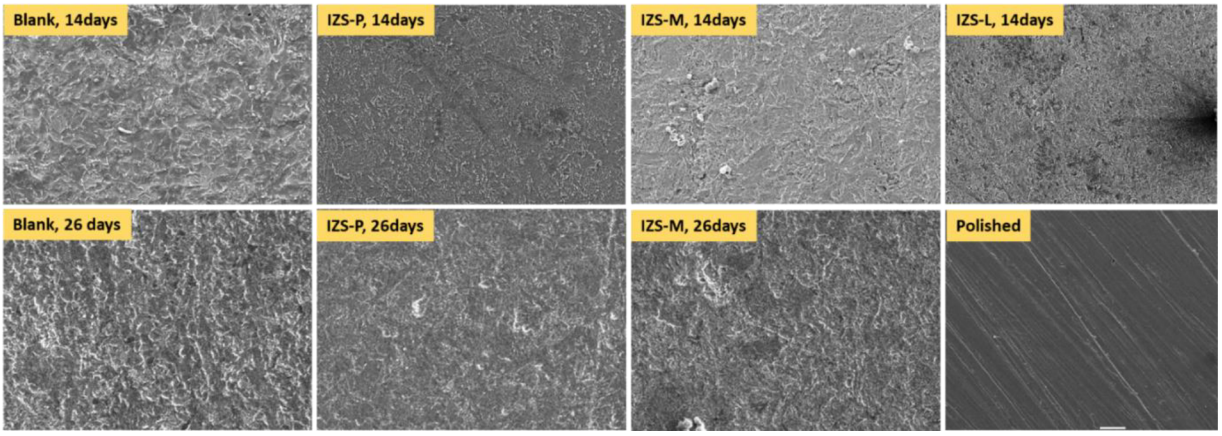

Figure 10. SEM images of mild steel, polished and in the absence and presence of IZSs after 14 days and 26 days immersion in ASW at 301 K.

https://doi.org/10.1021/acsomega.3c00366
ACS Omega 2023, 8, 24797−24812

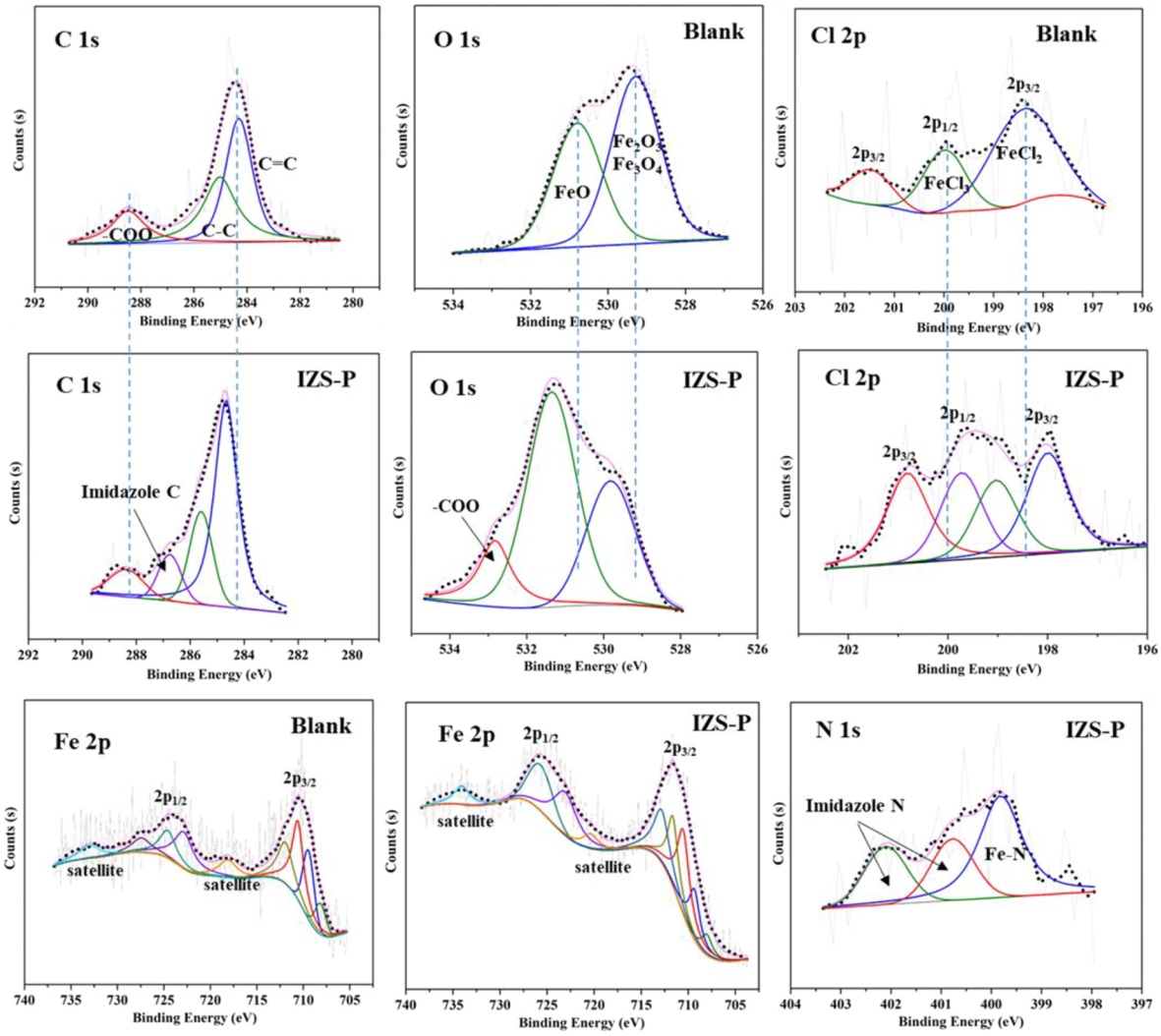

Figure 11. XPS deconvoluted profiles of C 1s, N 1s O 1s, and Cl 2p and (d) Fe 2p for mild steel in the absence (blank) and presence of IZS-P in ASW (smoothed, fitted, raw data).

amount of oxygen (26.81%) compared to that in the presence of inhibitors: IZS-P (0.92%), IZS-M (0.83%), and IZS-L (3.45%). This indicates that in the case of blank, the existing high-oxide layer on the mild steel surface is due to pronounced corrosion in ASW. Besides the low-oxide layer in the presence of inhibitors, the presence of nitrogen and surface also supported the IZS-P and IZS-M participation in the formation of a passive film on the mild steel surface.

XPS Analysis. The composition of mild steel surface was analyzed by XPS techniques in the absence and presence of IZS-P in ASW. The wide spectra of mild are depicted in Figure S8. The deconvoluted spectra of high-resolution peaks C 1s, N 1s, O 1s, Cl 2p, and Fe 2p are shown in Figure 11.

C 1s spectra of the blank show one prominent peak that is deconvoluted into three components. The peaks at 284.3, 285.20, and 288.48 eV defined the presence of C═C, C−C, and −O−C═O, respectively.[50] However, the C 1s spectra in the presence of IZS-P show a single broad peak that is deconvoluted into seven components. The peak presence at 283.37 and 284.6 eV reveals the C−H and C−C species.[51] A significant percentage peaks at 285.68 and 286.70 eV are related to the imidazole C-atom. In addition, the peak at 287.94 eV is related to adsorbed imidazole C-atom.[52] The last peak at high energy 288.36 eV shows the carboxylic group (−O−C═O). The presence of additional imidazole peaks and difference spectrum compared to blank reveals the presence of adsorbed IZS-P film on the mild steel surface.

N 1s spectra of IZS-P-inhibited mild steel was deconvoluted into four main peaks. The peaks at 395.98 and 397.85 eV correspond to the chemisorbed inhibitor-metal bond (Fe-N).[53] Another two peaks at 399.72 and 401.41 eV are related to imidazole nitrogen.[54] The N 1s spectra further support the participation of IZS-P in the passive film of mild steel.

O 1s spectra of blank deconvoluted into two main peaks. The peak at 529.28 eV is related to ferric oxides (Fe_2O_3, Fe_3O_4) and the peak at 530.79 eV corresponds to ferrous oxide (FeO).[55,56] This indicates that the oxide layer covered the mild steel surface. In the presence of IZS-P, the O 1s spectra were deconvoluted into four components. The presence of an additional peak at 532.49 eV may be related to the adsorbed water molecule[57] or can also correspond to the carboxylic group (−O−C═O) of IZS-P.[58] In addition, the presence of a Cl 2p peak is also related to the formation of a passive film on the metal surface. In both blank and IZS-P, the peak is deconvoluted into three components, which signify the

https://doi.org/10.1021/acsomega.3c00366
ACS Omega 2023, 8, 24797−24812

Table 6. Quantum Chemical Parameters Derived from the B3LYP/6-31G(d,p) Method[a]

parameters→ inhibitors↓	phase (G or A)*	E_{HOMO} (eV)	E_{LUMO} (eV)	ΔE (eV)	η (eV)	χ (eV)	ΔE_1 (eV)	ΔE_2 (eV)	ΔN	μ (Debye)
IZS-L	G	−5.1269	−2.5358	2.5911	1.2955	3.8314	2.5392	3.3799	0.3815	12.674
	A	−5.6311	−0.0993	5.5318	2.7659	2.8652	4.9757	3.8841	0.3534	14.3201
IZS-P	G	−4.6499	−3.4531	1.1968	0.5984	4.0515	1.6219	2.9029	0.6421	14.4772
	A	−5.2006	−0.2468	4.9538	2.4769	2.7237	4.8282	3.4536	0.4232	19.1266
IZS-M	G	−5.1908	−2.5625	2.6283	1.3142	3.8767	2.5125	3.4438	0.3589	13.4560
	A	−5.7119	−0.1061	5.6058	2.8029	2.9090	4.9689	3.9649	0.3409	15.2416

[a]*G = Gaseous, *A = Aqueous.

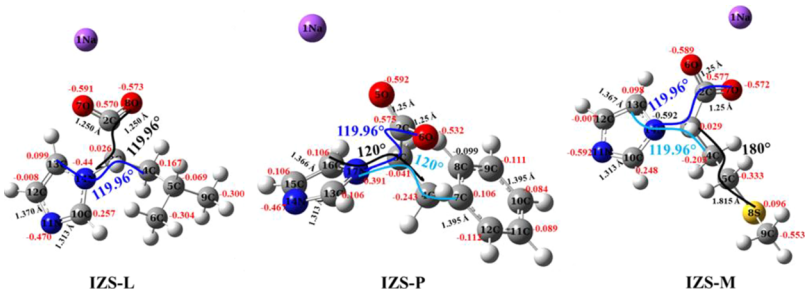

Figure 12. Optimized structure with atomic charges, bond lengths, and dihedral angle of IZS molecules.

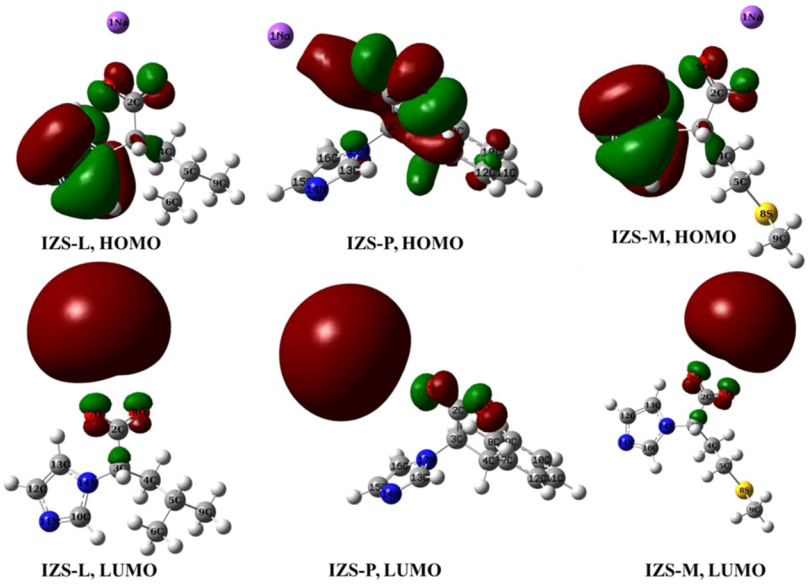

Figure 13. HOMO and LUMO structures of IZS inhibitor molecules.

presence of ferrous and ferric chlorides ($FeCl_2$ and $FeCl_3$) in the passive film.[58,59]

Fe 2p spectra of inhibited and uninhibited mild steel consist of double peak profiles as Fe $2p_{3/2}$ and Fe $2p_{1/2}$. The spectra of Fe $2p_{3/2}$ were deconvoluted into four components in blank and five components in the presence of IZS-P. The first two peaks in both cases in the range of 708.01 to 709.44 eV are related to Fe^{+2} species (FeO and $FeCl_2$).[60] The next two peaks in blank and three peaks in IZS-P are in the range of 710.54 to 712.83 eV corresponding to Fe^{+3} species: Fe_2O_3, FeOOH, and $FeCl_3$.[61,62] The presence of satellite peaks at 718.11 eV (blank) and 720.38 eV (IZS-P) are characteristic of the presence of Fe^{+3} oxide species.[62] The spectra of Fe $2P_{1/2}$ were deconvoluted into three (722.86, 724.57 and 727.40 eV) in blank and two (723.08 and 725.69 eV) components in the presence of IZS-P, which shows the presence of Fe^{+2} and Fe^{+3} oxide species.[62]

Corrosive Solution Analysis. The interaction of IZS molecules with dissolved iron as well as the change in corrosive solution after corrosion were analyzed by measuring the conductivity, pH, and analysis of the UV−visible spectra, as shown in Figure S9. The analysis was carried out at lower (2.1 mmol L^{-1}), optimum (6.3 mmol L^{-1}), and higher (10.5 mmol L^{-1}) inhibitor concentrations to compare with the results of inhibition performance; see Figure 2. It was found that with the mixing of inhibitors, the pH decreased compared to pure ASW (pH 8.2), which further decreases with increasing inhibitor concentrations in pure inhibitor solutions (IZS-L, IZS-P, and IZS-P) and after 24 h immersion of mild steel (IZS-L-MS, IZS-P-MS, and IZS-P-MS). The optimum concentration of pure effective inhibitors, IZS-M and IZS-P, show the lowest solution conductivity (Figure S9a). It concludes that at low and high inhibitor concentrations, the inhibitor molecules enhance the electrolyte conductivity, resulting in lower

https://doi.org/10.1021/acsomega.3c00366
ACS Omega 2023, 8, 24797−24812

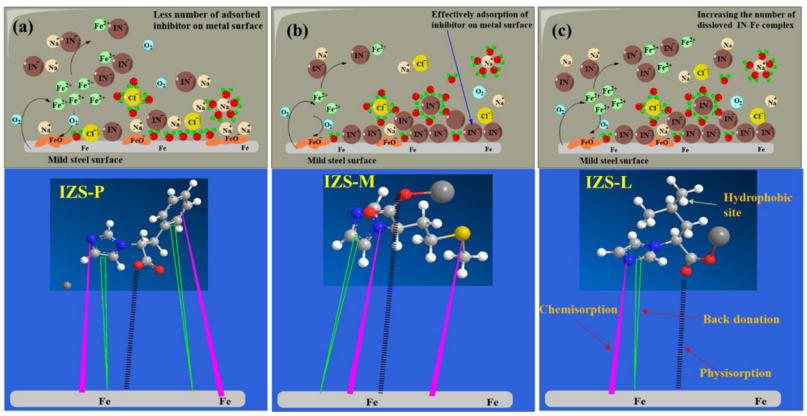

Figure 14. Systematic representation of the corrosion inhibition at lower (a), moderate (optimum) (b), and higher (c) inhibitor concentrations. The adsorption model of IZSs on mild steel surface.

inhibition efficiency (see Figure 2). Hence, the conductivity measurement suggests the potential inhibitor concentration and saves time to find out the most effective (optimum) inhibitor concentration.

In Figure S9b,c, the UV−visible spectra show similar spectra for the pure inhibitors of IZS-L and IZS-P and after corrosion (IZS-L-MS and IZS-P-MS), indicating that these inhibitors do not form the inhibitor-metal complex. However, the spectra of IZS-M-MS (after corrosion) (Figure S9c) show two new peaks at 255 nm (at 2.1 mmol L^{-1}) and 252 nm (at 6.3 mmol L^{-1}), signifying the formation of an inhibitor-metal complex.[63] It may cause an increase of solution conduction at 6.3 mmol L^{-1} concentration (Figure S9a) compared to the other two inhibitors. Hence, the results show that the greater interaction of IZS-M with the dissolved metal and enhancing the conductivity of the corrosive solution may be responsible for the poor inhibition performance of IZS-M at longer immersion times (Figure 5) and high temperatures (Figure 7) compared to IZS-P.

DFT Study. DFT is the most advanced computational technique to elucidate the electronic reactivity of inhibitor molecules. The calculated DFT parameters are shown in Table 6. In the optimized structure (Figure 12), the dihedral angle is close to 120° among all three moieties: imidazole ring, carboxyl group, and substituents (isobutyl in IZS-L, benzylic group in IZS-P, and ethyl methyl sulfide group). Hence, molecules are not completely flat, but they can interact with highly negatively charged atoms (O and N) and π-bond electrons of rings. In the carboxylic group, both the C−O bond are in an equal distance in all three inhibitors, showing that the negatively charged electrons are equally delocalized between both the C−O bonds. The delocalized structure can form a chelate structure with the metal surface.[64]

Figure 13, shows the structure of the highest occupied molecular orbital (HOMO) and the lowest unoccupied molecular orbital (LUMO). HOMOs are the molecular sites that can donate electrons to the metal vacant d-orbital, whereas LUMOs are electron-accepting sites through which molecules can accept lone-pair electrons from the iron. Figure 13, observes that HOMO is localized mainly on the imidazole moiety and some extend around the carboxylic group in IZS-L and IZS-M, whereas in IZS-P, the HOMOs are localized around the carboxylic group and adjacent carbon of rings (3C and 4C that have negative Mulliken charge). LUMOs are distributed around the carboxylic group and sodium ion. Hence, the carboxylic group plays a major role in donating as well as accepting electrons, leading to a strong interaction with the metal surface.[65]

As known, the organic inhibitor mainly adsorbs on the metallic surface through the electron-donating and electron-accepting mechanisms, which means interaction of frontier molecular orbitals (HOMO and LUMO). The high value of E_{HOMO} signifies that the electron of the outer shell is loosely bonded with a nucleus that can easily donate. In contrast, low values of E_{LUMO} signify that the molecule orbital have a high tendency to accept electrons that lead to reducing its nuclear charge.[66] From Table 5, in both gaseous and aqueous phases, the electron donation order is IZS-P > IZS-L > IZS-M and the electron acceptance order is IZS-P > IZS-M > IZS-L. Hence, IZS-P has greater electron-donating as well as electron-accepting capabilities. The energy gap (ΔE) between HOMO and LUMO is an important parameter to determine the inhibition performance of the inhibitor molecule. The lower ΔE value indicates a greater capacity of the inhibitor molecule interaction with the metal surface. From the results, IZS-P has the lowest ΔE, indicating a greater capability to interact with the metal surface, whereas the ΔE values do not much differ in the case of IZS-L and IZS-M. Furthermore, to elucidate the electron donation and acceptance between the metal IZSs, the energy level of the inhibitor has been compared with the energy level of Fe. From the energy of HOMO and LUMO, a two-energy gap has been calculated by the following equations:

$$\Delta E_1 = E_{LUMO(inhibitor)} - E_{HOMO(Fe)} \quad (13)$$

$$\Delta E_2 = E_{LUMO(Fe)} - E_{HOMO(inhibitor)} \quad (14)$$

The E_{HOMO} (−5.075 eV) and E_{LUMO} (−1.747 eV) of Fe (110) lattice plane were calculated by Huang et al. using the five atoms of Fe.[28] From the results, in a gaseous state, $\Delta E_1 < \Delta E_2$; this indicates that the interaction between E_{LUMO} of IZSs and E_{HOMO} of Fe was dominant over the interaction between E_{LUMO} of Fe and E_{HOMO} of IZSs, which means, IZSs can effectively accept electrons from metal d-orbitals, whereas in the aqueous phase, the results were reversed: $\Delta E_1 > \Delta E_2$. This shows that IZSs effectively donate electrons to Fe d-orbitals. Moreover, compared to the gaseous phase, the ΔE is slightly high in the aqueous phase indicating that the interaction of water molecule slows down the inhibitor-metal interaction.

https://doi.org/10.1021/acsomega.3c00366
ACS Omega 2023, 8, 24797−24812

Finally, the fraction of electron transfers and dipole moment are related to the inhibition effect of the inhibitors. The higher values of ΔN signify the greater electron transfer, that is, greater interaction with the metal surface. The results show that IZS-P exhibits a significantly high inhibition effect compared to IZS-L and IZS-M. Similar to ΔN, the high dipole moment indicates the capability of the inhibitor molecule to replace the water molecule from the metal surface.[67] In all inhibitors, the dipole moment is greater than the water molecule (1.82 Debye) in both the gaseous and aqueous phases, revealing that IZSs molecules can expel the water molecule and form a bond with the metal. The order of ΔN is IZS-P > IZS-M > IZS-L. Hence along with E_{LUMO} and ΔE_1, ΔN also supported the electrochemical results.

■ MECHANISM OF CORROSION INHIBITION

The experimental, surface, and DFT results disclosed that IZSs inhibit mild steel corrosion through an adsorption mechanism. The DFT results (Figure 13) show that IZS inhibitor molecules have several adsorption sites, and through this, IZSs interact with Fe d-orbitals and form chemical bonds, as shown in Figure 14d. The XPS results further supported the chemical interaction between IZSs and metal surfaces that disclosed the inhibitor adsorption mechanism. Besides, the electrochemical results reveal that IZSs may interact with the dissolved iron and adsorbed inhibitor molecules in corrosive solution, resulting in poor or negative inhibition performance at lower and higher inhibitor concentrations (Figure 2). The poor inhibition efficiency at lower and higher inhibitor concentrations may be due to higher conductivity of inhibitor solution; see Figure S9.[68] Combining all results, it can be concluded that the inhibitor molecule has competitive interaction between the metal surface and dissolved ions (iron and inhibitor). (a) At lower inhibitor concentration, the high solution conductivity compared to moderate concentration (Figure S9a), inhibitor molecule may have more tendency to interact with dissolved iron compared to the metal surface (Figure 14a) or may be a smaller number of inhibitor molecules available to adsorb on metal surface, resulted show the poor or negative inhibition efficiency. (b) At optimum (moderate) inhibitor concentration, the inhibitor molecule could predominantly interact with the metal surface compared to dissolved iron (Figure 14b), resulting in effective inhibition efficiency. (c) At higher inhibitor concentration, the metal surface gets saturated with the adsorbed inhibitor molecule and the extra molecules of inhibitor may interact with dissolved ions and/or adsorbed inhibitors (Figure 14c), resulting in an increase in the solution conductivity (Figure S9a) and a decrease in the inhibition efficiency.

Moreover, the expected adsorption model of IZSs on mild steel is shown in Figure 14. Based on surface studies and DFT results, the studied IZSs inhibitor contains π-bond, imidazole nitrogen, and carboxylate group, and through this, IZSs can donate their lone pair and π-bond electrons to the vacant d-orbital (chemisorption) of Fe. Simultaneously, the vacant π-bond antibonding orbitals of the carboxylate group can accept the lone pair electron from Fe filled d-orbital (back donation), resulting in minimized charge on inhibitor surface and enhanced adsorption capability. The negatively charged carboxylate group and the lone pair of imidazole nitrogen can be polarized toward the positively charged mild steel surface, resulting in formation of weak van der Waals bonding with the mild steel surface (physisorption).[69] Moreover, the experimentally obtained inhibition performance results, IZS-P > IZS-M > IZS-L, can correlate with their structural difference of inhibitor molecules; see Figure 1. DFT results show the greater electron distribution over the benzylic group ($-CH_2Ph$) in IZS-P (Figure 13), revealing that the benzene ring having π-bond can donate an electron to the metal d-orbital as well as its vacant π-bond antibonding orbitals can accept electron for the metal orbital, resulting in IZS-P exhibiting the highest inhibition performance. In IZS-M, the methylthioethyl ($-CH_2CH_2SCH_3$) side group has a sulfur atom that can donate its lone pair to the metal orbital through the chemisorption mechanism. However, the poorest inhibition performance of IZS-L may be due to the hydrophobic nature of the isobutyl ($-CH_2CH(CH_3)_2$) side group that cannot act as an adsorption site in IZS-L. Hence, among the three substituents, the benzylic group has the highest adsorption capability.

■ CONCLUSIONS

In this work, three novel IZSs were synthesized and analyzed as corrosion inhibitors for mild steel in ASW. Based on experimental results and discussion, the major conclusions are the following:

1. IZSs inhibitors have been synthesized by single-step reaction with high yield, high atom economy, and low *E*-factor. The exact structure of synthesized inhibitors has been confirmed by FTIR and NMR spectroscopy.
2. The electrochemical results show that IZSs exhibited effective corrosion inhibition at moderate concentration. The effective inhibition at moderate concentration may be due to lower solution conductivity compared to low and high inhibitor concentrations. Among IZSs, IZS-P showed the highest inhibition efficiency (82.46%) and the order of inhibitor performance is IZS-P > IZS-M > IZS-L.
3. The effect of immersion time and temperature results show that the phenyl group containing IZS-P exhibits better inhibition performance compared to methionine sulfur substituent IZS-M. SEM and EDX results further supported the better inhibition effect of IZS-P compared to IZS-M.
4. The XPS and FTIR results suggested that π-bond and heteroatom (N, O) functional groups of IZS-P effectively interact with the metal surface, resulting in reduced mild steel corrosion through the formation of a passive inhibitor film.
5. The experimental results reveal that IZSs inhibit mild steel corrosion through the adsorption mechanism. IZS-P obeys the Langmuir adsorption isotherm and IZS-M obeys the Frumkin adsorption isotherm.
6. DFT results well supported the experimental results. DFT results show that the imidazole ring and carboxylic group of IZSs effectively participate in electron transfer between IZSs and mild steel.
7. The corrosion study results and DFT calculations well support each other in the order of inhibitor performance, IZS-P > IZS-M > IZS-L. The greater electron distribution around the benzene ring in IZS-P signified its highest inhibitor performance. Moreover, the methylthioethyl in IZS-M has an additional good adsorptive sulfur atom compared to the isobutyl-containing IZS-L.

https://doi.org/10.1021/acsomega.3c00366
ACS Omega 2023, 8, 24797−24812

■ ASSOCIATED CONTENT

Supporting Information

The Supporting Information is available free of charge at https://pubs.acs.org/doi/10.1021/acsomega.3c00366.

FTIR and NMR of synthesized inhibitors, OCP and LPR curves of inhibitor and uninhibited mild steel, fitted Temkin isotherm, EDX spectra, wide XPS spectra of mild steel, and pH-conductivity analysis and UV−visible spectra (PDF)

■ AUTHOR INFORMATION

Corresponding Authors

Mohammad F. Ridwan Zulkifli − *Faculty of Ocean Engineering Technology and Informatics, Universiti Malaysia Terengganu, 21030 Kuala Nerus, Malaysia*; Email: fakhratulz@umt.edu.my

Wan Mohd Norsani Bin Wan Nik − *Faculty of Ocean Engineering Technology and Informatics, Universiti Malaysia Terengganu, 21030 Kuala Nerus, Malaysia*; orcid.org/0000-0003-4521-0127; Phone: +6-09-668-3901; Email: niksani@umt.edu.my

Authors

Jiyaul Haque − *Faculty of Ocean Engineering Technology and Informatics, Universiti Malaysia Terengganu, 21030 Kuala Nerus, Malaysia; Department of Chemistry, Indian Institute of Technology, Banaras Hindu University, Varanasi 221005, India*

Nabilah Ismail − *Faculty of Science and Marine Environment, Universiti Malaysia Terengganu, 21030 Kuala Nerus, Malaysia*

Mumtaz A. Quraishi − *Department of Chemistry, Indian Institute of Technology, Banaras Hindu University, Varanasi 221005, India;* Present Address: King Fahd University of Petroleum and Minerals, Interdisciplinary Research Center for Advanced Materials, Dhahran 31261, Saudi Arabia; orcid.org/0000-0002-7822-0084

Mohd Sabri Mohd Ghazali − *Faculty of Science and Marine Environment, Universiti Malaysia Terengganu, 21030 Kuala Nerus, Malaysia*

Elyor Berdimurodov − *Faculty of Natural Science, Karshi State University, Karshi 180119, Uzbekistan*

Complete contact information is available at: https://pubs.acs.org/10.1021/acsomega.3c00366

Notes

The authors declare no competing financial interest.

■ ACKNOWLEDGMENTS

The authors would like to acknowledge the Malaysian government grant (FRGS/1/2021/STG05/UMT/01/1-Corrosion Inhibition) for supporting this research. Support from Marine Materials Research Group and Marine Corrosion SIG is really appreciated.

■ REFERENCES

(1) Koch, G.; Varney, J.; Thompson, N.; Moghissi, O.; Gould, M.; Payer, J. International measures of prevention, application, and economics of corrosion technologies study. *NACE Int.* **2016**, *216*, 2−3.

(2) ISO, E., 8044. Corrosion of Metals and Alloys: Basic Terms and Definitions; European Committee for Standardization (CEN): Brussels, Belgium, 1999.

(3) Mohana, K.; Badiea, A. Effect of sodium nitrite−borax blend on the corrosion rate of low carbon steel in industrial water medium. *Corros. Sci.* **2008**, *50*, 2939−2947.

(4) Karim, S.; Mustafa, C.; Assaduzzaman, M.; Islam, M. Effect of nitrate ion on corrosion inhibition of mild steel in simulated cooling water. *Chem. Eng. Res. Bull.* **2010**, *14*, 87−91.

(5) Refaey, S.; Abd El-Rehim, S.; Taha, F.; Saleh, M.; Ahmed, R. Inhibition of chloride localized corrosion of mild steel by PO43−, CrO42−, MoO42−, and NO2− anions. *Appl. Surf. Sci.* **2000**, *158*, 190−196.

(6) Stephenson, L.; Wills, S.; van den Heuvel, C.; Humphries, M.; Byard, R. W. Increasing use of sodium nitrite in suicides—an emerging trend. *Forensic Sci., Med., Pathol.* **2022**, *18*, 311−318.

(7) Bokati, K. S.; Dehghanian, C. Adsorption behavior of 1H-benzotriazole corrosion inhibitor on aluminum alloy 1050, mild steel and copper in artificial seawater. *J. Environ. Chem. Eng.* **2018**, *6*, 1613−1624.

(8) Hoseinzadeh, A.; Javadpour, S. Electrochemical, thermodynamic and theoretical study on anticorrosion performance of a novel organic corrosion inhibitor in 3.5% NaCl solution for carbon steel. *Bull. Mater. Sci.* **2019**, *42*, 188.

(9) Finšgar, M.; Petovar, B.; Xhanari, K.; Maver, U. The corrosion inhibition of certain azoles on steel in chloride media: Electrochemistry and surface analysis. *Corros. Sci.* **2016**, *111*, 370−381.

(10) Ivušić, F.; Lahodny-Šarc, O.; Ćurković, H. O.; Alar, V. Synergistic inhibition of carbon steel corrosion in seawater by cerium chloride and sodium gluconate. *Corros. Sci.* **2015**, *98*, 88−97.

(11) Ivušić, F.; Lahodny-Šarc, O.; Stojanović, I. Corrosion inhibition of carbon steel in saline solutions by gluconate, zinc sulphate and green clay eluate. *Tehnički vjesnik* **2014**, *21*, 107−114.

(12) Heydari, M.; Javidi, M. Corrosion inhibition and adsorption behaviour of an amido-imidazoline derivative on API 5L X52 steel in CO2-saturated solution and synergistic effect of iodide ions. *Corros. Sci.* **2012**, *61*, 148−155.

(13) Gao, Y.; Ward, L.; Fan, L.; Li, H.; Liu, Z. A study of the use of polyaspartic acid derivative composite for the corrosion inhibition of carbon steel in a seawater environment. *J. Mol. Liq.* **2019**, *294*, No. 111634.

(14) Gao, Y.; Li, H.; Zheng, Y.; Zhang, L.; Liu, Z. Application of polyaspartic acid derivative in circulating cooling water system with high concentration multiple. *J. Phys.: Conf. Ser.* **2020**, No. 012133.

(15) Chauhan, D. S.; Quraishi, M.; Nik, W. W.; Srivastava, V. Triazines as a potential class of corrosion inhibitors: Present scenario, challenges and future perspectives. *J. Mol. Liq.* **2021**, *321*, No. 114747.

(16) Mor, E.; Wrubl, C. Zinc gluconate as an inhibitor of the corrosion of mild steel in sea water. *Br. Corros. J.* **1976**, *11*, 199−203.

(17) Loto, R. T.; Fajobi, M.; Oluwole, O.; Loto, C. A. Corrosion inhibition effect of calcium gluconate on mild steel in artificial seawater. *Cogent Eng.* **2020**, *7*, No. 1712155.

(18) Gladkikh, N.; Makarychev, Y.; Maleeva, M.; Petrunin, M.; Maksaeva, L.; Rybkina, A.; Marshakov, A.; Kuznetsov, Y. Synthesis of thin organic layers containing silane coupling agents and azole on the surface of mild steel. Synergism of inhibitors for corrosion protection of underground pipelines. *Prog. Org. Coat.* **2019**, *132*, 481−489.

(19) Berdimurodov, E.; Kholikov, A.; Akbarov, K.; Guo, L.; Kaya, S.; Katin, K. P.; Verma, D. K.; Rbaa, M.; Dagdag, O.; Haldhar, R. Novel gossypol−indole modification as a green corrosion inhibitor for low−carbon steel in aggressive alkaline−saline solution. *Colloids Surf., A* **2022**, *637*, No. 128207.

(20) Hassan, N.; Ramadan, A. M.; Khalil, S.; Ghany, N. A. A.; Asiri, A. M.; El-Shishtawy, R. M. Experimental and computational investigations of a novel quinoline derivative as a corrosion inhibitor for mild steel in salty water. *Colloids Surf., A* **2020**, *607*, No. 125454.

(21) Chauhan, D. S.; Mouaden, K. E.; Quraishi, M.; Bazzi, L. Aminotriazolethiol-functionalized chitosan as a macromolecule-based

bioinspired corrosion inhibitor for surface protection of stainless steel in 3.5% NaCl. *Int. J. Biol. Macromol.* **2020**, *152*, 234−241.
(22) Al-Joborry, N. M.; Kubba, R. M. Theoretical and Experimental Study for Corrosion Inhibition of Carbon Steel in Salty and Acidic Media by A New Derivative of Imidazolidine 4-One. *Iraqi J. Sci.* **2020**, *61*, 1842−1860.
(23) Jawich, M. W.; Oweimreen, G.; Ali, S. A. Heptadecyl-tailed mono-and bis-imidazolines: A study of the newly synthesized compounds on the inhibition of mild steel corrosion in a carbon dioxide-saturated saline medium. *Corros. Sci.* **2012**, *65*, 104−112.
(24) Curkovic, H. O.; Stupnisek-Lisac, E.; Takenouti, H. The influence of pH value on the efficiency of imidazole based corrosion inhibitors of copper. *Corros. Sci.* **2010**, *52*, 398−405.
(25) Haque, J.; Srivastava, V.; Quraishi, M. A.; Chauhan, D. S.; Lgaz, H.; Chung, I.-M. Polar group substituted imidazolium zwitterions as eco-friendly corrosion inhibitors for mild steel in acid solution. *Corros. Sci.* **2020**, *172*, No. 108665.
(26) Srivastava, V.; Haque, J.; Verma, C.; Singh, P.; Lgaz, H.; Salghi, R.; Quraishi, M. Amino acid based imidazolium zwitterions as novel and green corrosion inhibitors for mild steel: Experimental, DFT and MD studies. *J. Mol. Liq.* **2017**, *244*, 340−352.
(27) Stupnišek-Lisac, E.; Božić, A. L.; Cafuk, I. Low-toxicity copper corrosion inhibitors. *Corrosion* **1998**, *54*, 713−720.
(28) Bao, W.; Wang, Z.; Li, Y. Synthesis of chiral ionic liquids from natural amino acids. *J. Org. Chem.* **2003**, *68*, 591−593.
(29) Altava, B.; Barbosa, D. S.; Burguete, M. I.; Escorihuela, J.; Luis, S. V. Synthesis of new chiral imidazolium salts derived from amino acids: their evaluation in chiral molecular recognition. *Tetrahedron: Asymmetry* **2009**, *20*, 999−1003.
(30) Testing, A. S. F. Materials. In *Standard practice for the preparation of substitute ocean water*; ASTM International, 2013.
(31) Frisch, M.; Trucks, G. W.; Schlegel, H. B.; Scuseria, G. E.; Robb, M. A.; Cheeseman, J. R.; Scalmani, G.; Barone, V.; Mennucci, B.; Petersson, G. *Gaussian 09, revision D. 01*; Gaussian, Inc.: Wallingford CT, 2009.
(32) Kokalj, A.; Kovačević, N. On the consistent use of electrophilicity index and HSAB-based electron transfer and its associated change of energy parameters. *Chem. Phys. Lett.* **2011**, *507*, 181−184.
(33) Beda, R.; Niamien, P.; Bilé, E. A.; Trokourey, A. Inhibition of aluminium corrosion in 1.0 M HCl by caffeine: experimental and DFT studies. *Adv. Chem.* **2017**, *2017*, No. 6975248.
(34) Cao, Z.; Tang, Y.; Cang, H.; Xu, J.; Lu, G.; Jing, W. Novel benzimidazole derivatives as corrosion inhibitors of mild steel in the acidic media. Part II: Theoretical studies. *Corros. Sci.* **2014**, *83*, 292−298.
(35) Juárez, E. G.; Mena-Cervantes, V. Y.; Vazquez-Arenas, J.; Flores, G. P.; Hernandez-Altamirano, R. Inhibition of CO2 corrosion via sustainable geminal zwitterionic compounds: effect of the length of the hydrocarbon chain from amines. *ACS Sustainable Chem. Eng.* **2018**, *6*, 17230−17238.
(36) Sheldon, R. A. Fundamentals of green chemistry: efficiency in reaction design. *Chem. Soc. Rev.* **2012**, *41*, 1437−1451.
(37) Lahodny-Šarc, O.; Popov, S. Corrosion inhibition of mild steel in sodium gluconate-borate solutions. *Surf. Coat. Technol.* **1988**, *34*, 537−547.
(38) Obot, I. B.; Onyeachu, I. B.; Umoren, S. A. Alternative corrosion inhibitor formulation for carbon steel in CO2-saturated brine solution under high turbulent flow condition for use in oil and gas transportation pipelines. *Corros. Sci.* **2019**, *159*, No. 108140.
(39) De Levie, R. The influence of surface roughness of solid electrodes on electrochemical measurements. *Electrochim. Acta* **1965**, *10*, 113−130.
(40) Luo, X.; Pan, X.; Yuan, S.; Du, S.; Zhang, C.; Liu, Y. Corrosion inhibition of mild steel in simulated seawater solution by a green eco-friendly mixture of glucomannan (GL) and bisquaternary ammonium salt (BQAS). *Corros. Sci.* **2017**, *125*, 139−151.
(41) Qiang, Y.; Zhang, S.; Tan, B.; Chen, S. Evaluation of Ginkgo leaf extract as an eco-friendly corrosion inhibitor of X70 steel in HCl solution. *Corros. Sci.* **2018**, *133*, 6−16.
(42) Haque, J.; Srivastava, V.; Chauhan, D. S.; Lgaz, H.; Quraishi, M. A. Microwave-induced synthesis of chitosan Schiff bases and their application as novel and green corrosion inhibitors: experimental and theoretical approach. *ACS Omega* **2018**, *3*, 5654−5668.
(43) Otmačić, H.; Stupnišek-Lisac, E. Copper corrosion inhibitors in near neutral media. *Electrochim. Acta* **2003**, *48*, 985−991.
(44) Rashid, K. H.; Khadom, A. A. 3-Methoxypropyl-amine as corrosion inhibitor for X80 steel in simulated saline water. *J. Mol. Liq.* **2020**, *319*, No. 114326.
(45) Langmuir, I. The constitution and fundamental properties of solids and liquids. Part I. Solids. *J. Am. Chem. Soc.* **1916**, *38*, 2221−2295.
(46) Trasatti, S. Acquisition and analysis of fundamental parameters in the adsorption of organic substances at electrodes. *J. Electroanal. Chem. Interfacial Electrochem.* **1974**, *53*, 335−363.
(47) Kokalj, A. Corrosion inhibitors: physisorbed or chemisorbed? *Corros. Sci.* **2022**, *196*, No. 109939.
(48) Zulkifli, F.; Yusof, M. S. M.; Khairul, W.; Rahamathullah, R.; Isa, M.; Nik, W. W. The effect of concentration of Lawsonia inermis as a corrosion inhibitor for aluminum alloy in seawater. *Adv. Phys. Chem.* **2017**, *2017*, No. 8521623.
(49) Balasubramaniam, R.; Kumar, A. R.; Dillmann, P. Characterization of rust on ancient Indian iron. *Curr. Sci.* **2003**, 1546−1555.
(50) Usman, B. J.; Gasem, Z. M.; Umoren, S. A.; Solomon, M. M. Eco-friendly 2-Thiobarbituric acid as a corrosion inhibitor for API 5L X60 steel in simulated sweet oilfield environment: Electrochemical and surface analysis studies. *Sci. Rep.* **2019**, *9*, 830.
(51) Ochoa, N.; Bello, M.; Sancristóbal, J.; Balsamo, V.; Albornoz, A.; Brito, J. L. Modified cassava starches as potential corrosion inhibitors for sustainable development. *Mater. Res.* **2013**, *16*, 1209−1219.
(52) Xue, G.; Dai, Q.; Jiang, S. Chemical reactions of imidazole with metallic silver studied by the use of SERS and XPS techniques. *J. Am. Chem. Soc.* **1988**, *110*, 2393−2395.
(53) Vanini, A. S.; Audouard, J.-P.; Marcus, P. The role of nitrogen in the passivity of austenitic stainless steels. *Corros. Sci.* **1994**, *36*, 1825−1834.
(54) Rezaei, A.; Hadian-Dehkordi, L.; Samadian, H.; Jaymand, M.; Targhan, H.; Ramazani, A.; Adibi, H.; Deng, X.; Zheng, L.; Zheng, H. Pseudohomogeneous metallic catalyst based on tungstate-decorated amphiphilic carbon quantum dots for selective oxidative scission of alkenes to aldehyde. *Sci. Rep.* **2021**, *11*, 4411.
(55) Bouanis, M.; Tourabi, M.; Nyassi, A.; Zarrouk, A.; Jama, C.; Bentiss, F. Corrosion inhibition performance of 2, 5-bis (4-dimethylaminophenyl)-1, 3, 4-oxadiazole for carbon steel in HCl solution: Gravimetric, electrochemical and XPS studies. *Appl. Surf. Sci.* **2016**, *389*, 952−966.
(56) Hashim, N. Z. N.; Kassim, K.; Zaki, H. M.; Alharthi, A. I.; Embong, Z. XPS and DFT investigations of corrosion inhibition of substituted benzylidene Schiff bases on mild steel in hydrochloric acid. *Appl. Surf. Sci.* **2019**, *476*, 861−877.
(57) Wang, D.; Yue, Y.; Xie, Z.; Mi, T.; Yang, S.; McCague, C.; Qian, J.; Bai, Y. Chloride-induced depassivation and corrosion of mild steel in magnesium potassium phosphate cement. *Corros. Sci.* **2022**, *206*, No. 110482.
(58) Chastain, J.; King, R. C., Jr. *Handbook of X-ray photoelectron spectroscopy*; Perkin-Elmer Corporation, 1992; Vol. *40*, p 221.
(59) Zhang, Y.; Pan, Y.; Li, P.; Zeng, X.; Guo, B.; Pan, J.; Hou, L.; Yin, X. Novel Schiff base-based cationic Gemini surfactants as corrosion inhibitors for Q235 carbon steel and printed circuit boards. *Colloids Surf., A* **2021**, *623*, No. 126717.
(60) Grosvenor, A.; Kobe, B.; Biesinger, M.; McIntyre, N. Investigation of multiplet splitting of Fe 2p XPS spectra and bonding in iron compounds. *Surf. Interface Anal.* **2004**, *36*, 1564−1574.
(61) Biesinger, M. C.; Payne, B. P.; Grosvenor, A. P.; Lau, L. W.; Gerson, A. R.; Smart, R. S. C. Resolving surface chemical states in

https://doi.org/10.1021/acsomega.3c00366
ACS Omega 2023, 8, 24797−24812

XPS analysis of first row transition metals, oxides and hydroxides: Cr, Mn, Fe, Co and Ni. *Appl. Surf. Sci.* **2011**, *257*, 2717−2730.
(62) Di Castro, V.; Ciampi, S. XPS study of the growth and reactivity of Fe/MnO thin films. *Surf. Sci.* **1995**, *331*, 294−299.
(63) Li, D.; Zhang, P.; Guo, X.; Zhao, X.; Xu, Y. The inhibition of mild steel corrosion in 0.5 MH 2 SO 4 solution by radish leaf extract. *RSC Adv.* **2019**, *9*, 40997−41009.
(64) Azócar, M. I.; Gómez, G.; Levín, P.; Paez, M.; Muñoz, H.; Dinamarca, N. Antibacterial behavior of carboxylate silver (I) complexes. *J. Coord. Chem.* **2014**, *67*, 3840−3853.
(65) Luo, X.; Dong, C.; Xi, Y.; Ren, C.; Wu, J.; Zhang, D.; Yan, X.; Xu, Y.; Liu, P.; He, Y.; Li, X. Computational simulation and efficient evaluation on corrosion inhibitors for electrochemical etching on aluminum foil. *Corros. Sci.* **2021**, *187*, No. 109492.
(66) Zhang, X.; Kang, Q.; Wang, Y. Theoretical study of N-thiazolyl-2-cyanoacetamide derivatives as corrosion inhibitor for aluminum in alkaline environments. *Comput. Theor. Chem.* **2018**, *1131*, 25−32.
(67) Singh, R.; Prasad, D.; Safi, Z.; Wazzan, N.; Guo, L. De-scaling, experimental, DFT, and MD-simulation studies of unwanted growing plant as natural corrosion inhibitor for SS-410 in acid medium. *Colloids Surf., A* **2022**, *649*, No. 129333.
(68) Reza, M.; Shafiee, M.; Moloudi, R.; Ghashang, M. ZnO nanopowder: an efficient catalyst for the preparation of 2, 4, 6-triaryl pyridines under solvent-free condition. *APCBEE Proc.* **2012**, *1*, 221−225.
(69) Belarbi, Z.; Farelas, F.; Singer, M.; Nešić, S. Role of amines in the mitigation of CO2 Top of the Line Corrosion. *Corrosion* **2016**, *72*, 1300−1310.

https://doi.org/10.1021/acsomega.3c00366
ACS Omega 2023, 8, 24797−24812